SAND2020-1989C

THE EFFECTS OF BOUNDARY CONDITIONS ON DAMAGE POTENTIAL FROM SHOCKS

Vit Babuška, Carl Sisemore, Robert Flores
Sandia National Laboratories*
Albuquerque, NM 87185

ABSTRACT

Component testing is always performed independently of the actual system in which the component is intended to be employed. As a result, the boundary interface stiffness and impedance in a component level test frequently differ from the system level conditions. Modal analysis can be used to identify differences between the test condition and the as-installed system level conditions. However, damage type quantities of interest are better for determining the effects of boundary condition differences in a test. This paper presents the results of experimental shock testing using two different boundary conditions comparing component damage. The basic Box Assembly with Removable Component (BARC) structure was modified with external components to evaluate system damage due to shock excitation under different boundary conditions. The results showed that shock damage sensitivity to boundary conditions depends on the relative flexibility between the component and the structure to which it is attached. Peak acceleration may not be a good quantity of interest for estimating damage sensitivity if there is a relatively flexible element in the load path. Relative deformational quantities of interest are likely to be more predictive, but their utility depends on good quality data since accelerations must be integrated and that can introduce errors.

I. INTRODUCTION

Component tests are performed to identify potential in-service failure modes and demonstrate robustness (i.e., the ability to survive and function) to in-service environments. It is difficult, and in most cases not possible, to test a full-scale assembly to determine how a component performs in shock and vibration environments. Ideally, component tests are performed with a test fixture that represents the boundary conditions the component would see within the assembly. However, there will be some variance between the fixture's impedance and the actual assembly's impedance. Therefore, we want to assess how boundary conditions affect damage potential or component robustness. In this paper we focus on drop shock environments. Specifically, we subjected a modified Box Assembly with Removable Component (BARC) structure [1],[2] called the BARBECUE - Box and Removable Bridge with External Components Under Evaluation to a series of shocks on a drop table. Failure modes and damage were evaluated. The responses also were evaluated with a variety of Quantities of Interest (QoIs) to identify which ones provide insight into boundary condition sensitivity to shock damage.

The paper is organized into five sections. The next section describes the BARBECUE structure and its two variants – the BRIDGE and BOB (Bridge on Box). Section 3 summarizes the quantities of interest used to assess damage and damage potential of the shock environments. Damage was defined as visible deformation or fracture. The drop shock tests are discussed in Section 4. The test results are described in Section 5 and Section 6 contains conclusions about boundary condition sensitivity and damage potential. The main conclusions are: 1) damage sensitivity depends on geometry and the flexibility of components in the load path as much as on the boundary conditions; 2) if there are flexible components in the load path, the accelerations may be high on the shock sensitive component but that may be due to non-damaging rigid body motion; 3) relative deformational quantities of interest are likely to be more predictive, but their utility depends on good measurements since accelerations must be integrated and that can introduce errors.

Sandia National Laboratories is a multimission laboratory managed and operated by National Technology & Engineering Solutions of Sandia, LLC, a wholly owned subsidiary of Honeywell International Inc., for the U.S. Department of Energy's National Nuclear Security Administration under contract DE-NA0003525.

II. BARBECUE TESTBED

Components and Configurations

The BARBECUE testbed, shown in Figure 1, consists of the BARC box (Figure 2), with a bridge component (Figure 3) on two C-channels (Figure 5) and two towers (Figure 4) with changeable collar weights. The components of interest are the bridge and the towers. We are interested in the environments at the base of the bridge's C-channels and the effect that the presence or absence of the BARC box has on the failure modes of the bridge and towers.

The BARC box is a 6" by 6" by 3" square with a thickness of 1/4". The part is made of T6061 aluminum. There is a single cut on top of the box that is 1/2" wide. In addition to this cut there are a total of 18 holes in the BARC box. Six of the holes are at the base of the BARC box, opposite to the side with the 1/2" cut. These six holes are to mount the BARC box to a fixture. The remaining holes in the BARC box are on its topside, where the 1/2" cut is present. These holes are for connecting two aluminum C-channels that support the bridge on the BARC box. There are also four small holes, broken up into pairs near the aluminum C-channel connection holes. These four holes are for accelerometers. The hole spacing is compatible with Endevco 7274 or 7270 accelerometers.

Figure 1: BARBECUE Testbed (BOB Configuration)

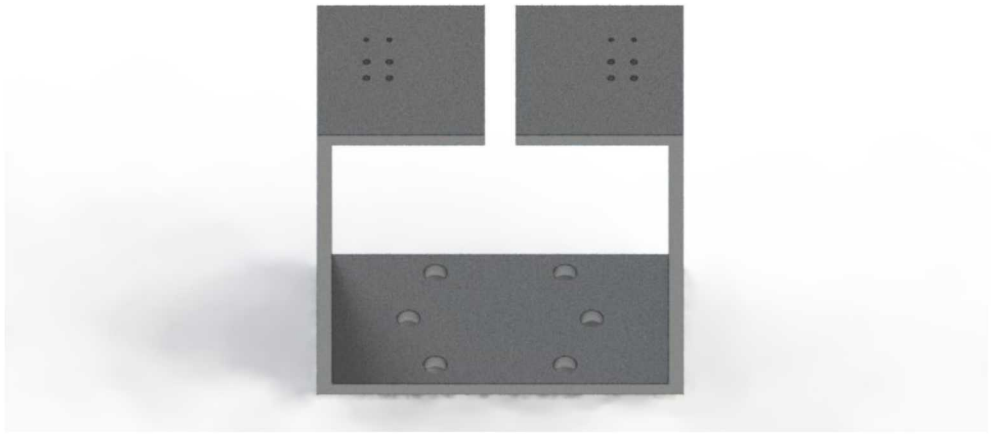

Figure 2: Box Assembly with Removable Component (BARC) Box

The bridge, shown in Figure 3, is an additively manufactured (AM) piece made from 316 L stainless steel. It is different from the bridge component in the standard BARC testbed. Like the standard BARC testbed, this bridge sits on two aluminum C-channels that are oriented asymmetrically. One of the C-channels faces in, along the length of the bridge and the other is oriented perpendicular to the inward facing one. This is the standard BARC orientation. The bridge is 5" long, 1" wide, and 1/8" thick. There are a total of fourteen holes and two slots. The holes on each end are for attaching the bridge to the aluminum C-channels. Two sets of three holes in triangular patterns are where the towers are attached. Two small holes in center are for an accelerometer (Endevco 7274 or 7270). There are four triangular holes through the thickness of the bridge. The triangular holes introduce a stress concentration zone in the bridge. These triangular holes could have only been made through additive manufacturing techniques. The two slots, which go through the main surface of the bridge, are just very large voids in the bridge, created to cause failure near the edges of the bridge.

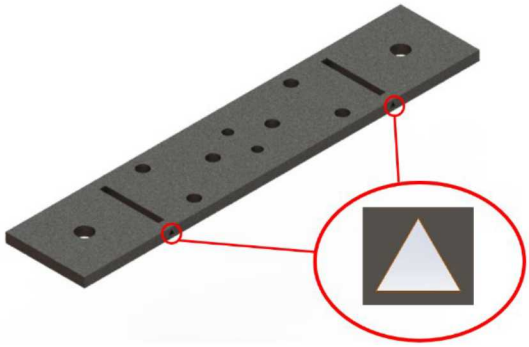

Figure 3: AM 316L Stainless Steel Bridge

The towers (Figure 4) also were additively manufactured. They are 2" tall with a 1" diameter cylindrical base that is 1/8" thick; the rest of the tower has a diameter of 1/4". The important structural characteristic is the pattern of three elliptical holes near the root of the tower. The elliptical holes, like the triangular holes, could not have been made without using additive manufacturing techniques. They are intended to localize potential failure modes. The elliptical holes are 0.35" along the semi-major axis and 0.13" along the semi-minor axis. The towers are bolted to the bridge through the three holes in the cylindrical base. In addition, two holes at the tips of each tower are for accelerometers. The hole spacing is compatible with Endevco 7274 or 7270 accelerometers. Collar weights can be attached to the towers to tailor their modal properties.

Figure 4: AM 316L Stainless Steel Tower

Two configurations of the BARBECUE testbed were used in the drops shock tests. The first, designated BOB (Bridge on Box) is the configuration shown in Figure 1, with two collar weights. One of the collar weights, called the “Large Weight” (LW) is 1.75" in diameter, while the other is the “Small Weight (SW) and is 1" in diameter. The dimensions and mass properties of the collar weights are summarized in Table 1.

Table 1 Mass Properties of the Collar Weights

Weight	Diameter (in)	Thickness (in)	Material	Mass	Moment of Inertia (I_{xx}) [lb-in^2]	Moment of Inertia (I_{yy}) [lb-in^2]
Large (LW)	1.75	0.25	AISI 1215 Carbon Steel	138 g	0.065972	0.065309
Small (SW)	1.0	0.25	AISI 1026 Carbon Steel	32 g	0.005583	0.005416

The Large Weight was attached to the tower on the side of bridge where the C-channel faces in, along the length of the beam. The Small Weight was attached to the tower on the other side. This was the configuration for all but one test, in which the weights were reversed. The BARC box was attached to the test fixture. In this configuration the shock loads travel through the BARC box before reaching the bridge.

The second configuration was the BRIDGE configuration, illustrated in Figure 5. In this configuration the BRIDGE is attached to the test fixture without the BARC box. In this configuration, the shock loads are applied directly to the base of the C-channels.

The boundary conditions at the base of the bridge depend on whether the BARC box is present or not. In the BOB configuration the bridge is on a relatively compliant base and has flexible boundary conditions. In the BRIDGE configuration, the boundary conditions are rigid.

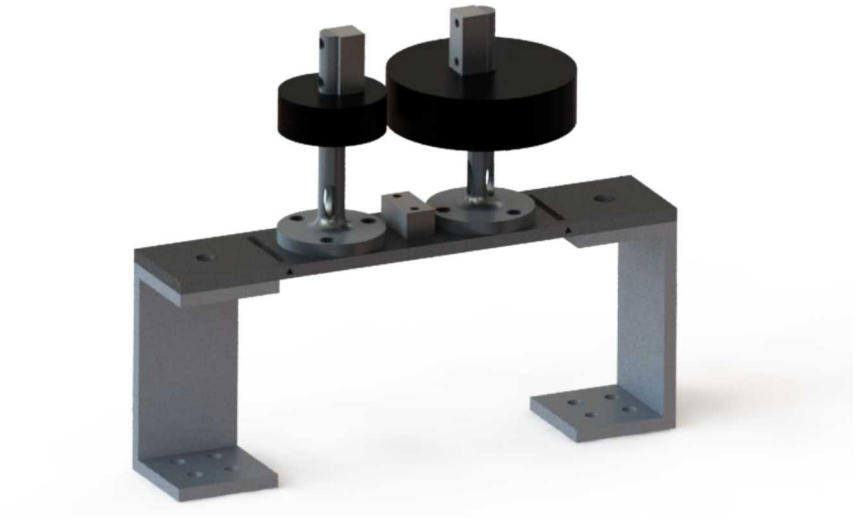

Figure 5: BRIDGE Configuration

Instrumentation

The structures were instrumented with five triaxial accelerometers as shown in Figure 6. Each tower was instrumented with a triaxial accelerometer as was the center of the bridge. Triaxial accelerometers were installed at the base of the bridge C-channels. In the BOB configuration they were on the BARC box. In the Bridge configuration they were on the fixture. The carriage was instrumented with an Endevco 7920A-100 single axis accelerometer.

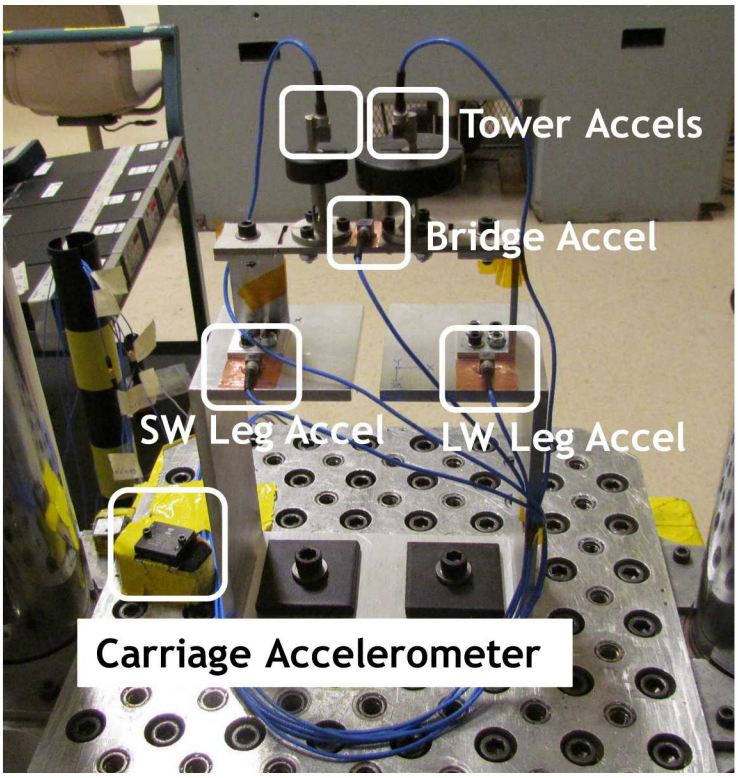

Figure 6 Instrumentation on the BOB Configuration

Modal Properties

The modal properties of both configurations were computed with ANSYS. The finite element model for both configurations used a fixed boundary condition. Weights and accelerometers were treated as rigid lump masses in the finite element models. No modal tests were performed so the ANSYS models were not validated, but the finite elements models were built using good modeling practices and accurate material properties. Therefore, we believe that the models are appropriate for a relative comparison of the modal properties of the two configurations.

The mode shapes for each of the two models generally are different; however, some mode shapes produced in each analysis were similar, as expected. Table 2 lists each mode shape that overlapped in each modal analysis study, with their respective frequencies, and descriptions of what is happening in that mode. Figure 7 through Figure 9 are three mode shapes used for visualization of the descriptions from Table 2.

Table 2: Mode Shape Comparison between BOB and BRIDGE Configurations

BOB			BRIDGE		
Mode	**Frequency (Hz)**	**Description**	**Mode**	**Frequency (Hz)**	**Description**
2	93	Box bending about Z-axis	1	166	Left bridge leg bending about Z-axis No deformation in bridge and towers
4	236	Box walls bend, close the box gap Bridge bending about X-axis	4	400	Bridge bending about X-axis Out-of-phase tower rigid motion
5	282	Left box arm X-axis motion Right tower torsion	3	326	Right tower torsion
7	323	Right tower bending about X-axis	6	547	Right bridge leg bending about X-axis Right tower bending about X-axis
8	389	Bridge bending about Z-axis	7	799	Left bridge leg bending about Z-axis Left tower rigid body motion
14	678	Left tower bending about X-axis	8	864	Left tower bending about X-axis
17	1017	Left tower torsion	9	1053	Left tower torsion Right tower bending about Z-axis Bridge twist
18	1261	Right side box bending about X-axis	10	1182	Left tower torsion Right tower bending about Z-axis Bridge twist
20	1481	Left box wall bending Complex bridge bending	11	1561	Bending of both bridge legs Bridge deformation Right tower bending about X-axis
22	1674	Left box wall bending Complex bridge bending	12	2211	Left bridge leg bending about Z-axis Right tower bending about X-axis
23	1834	Left side box top local flapping	13	2368	Bridge twist about Z-axis Right tower bending about z-axis
27	2514	Right box wall torsion about Y-axis Bridge twist about y-axis	14	3348	Left bridge leg bending Bridge twist on left side

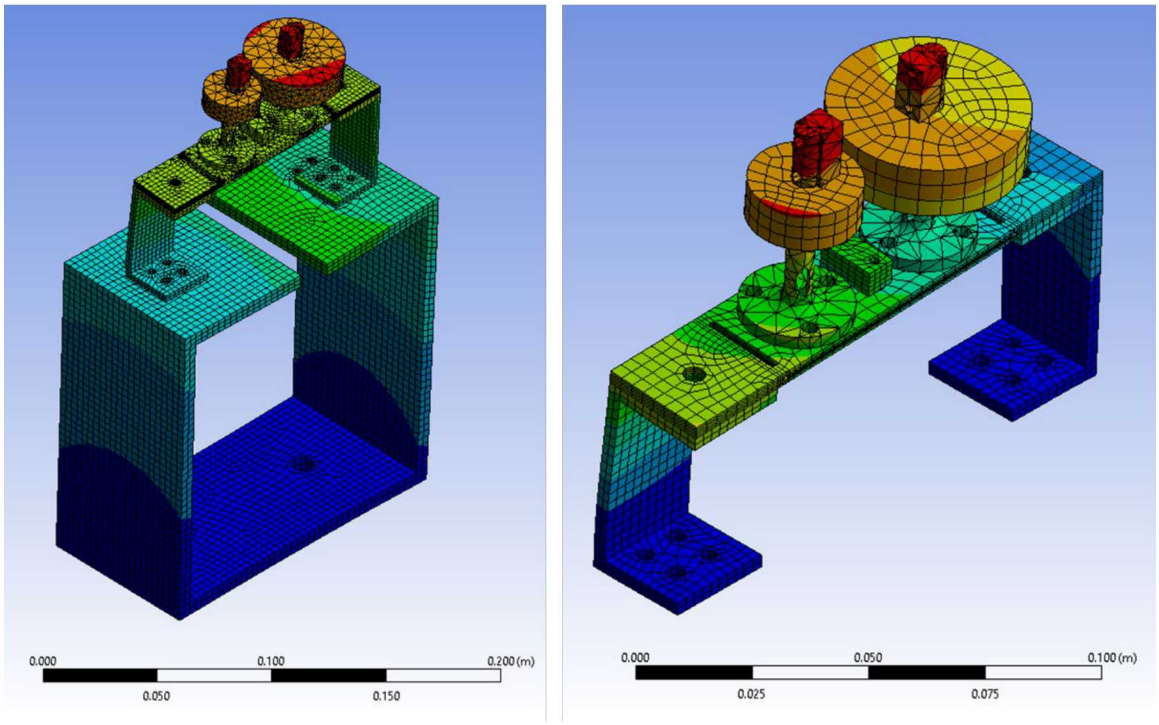

Figure 7: BOB Mode 2 [96 Hz] (left) and BRIDGE Mode 1 [166 Hz] (right)

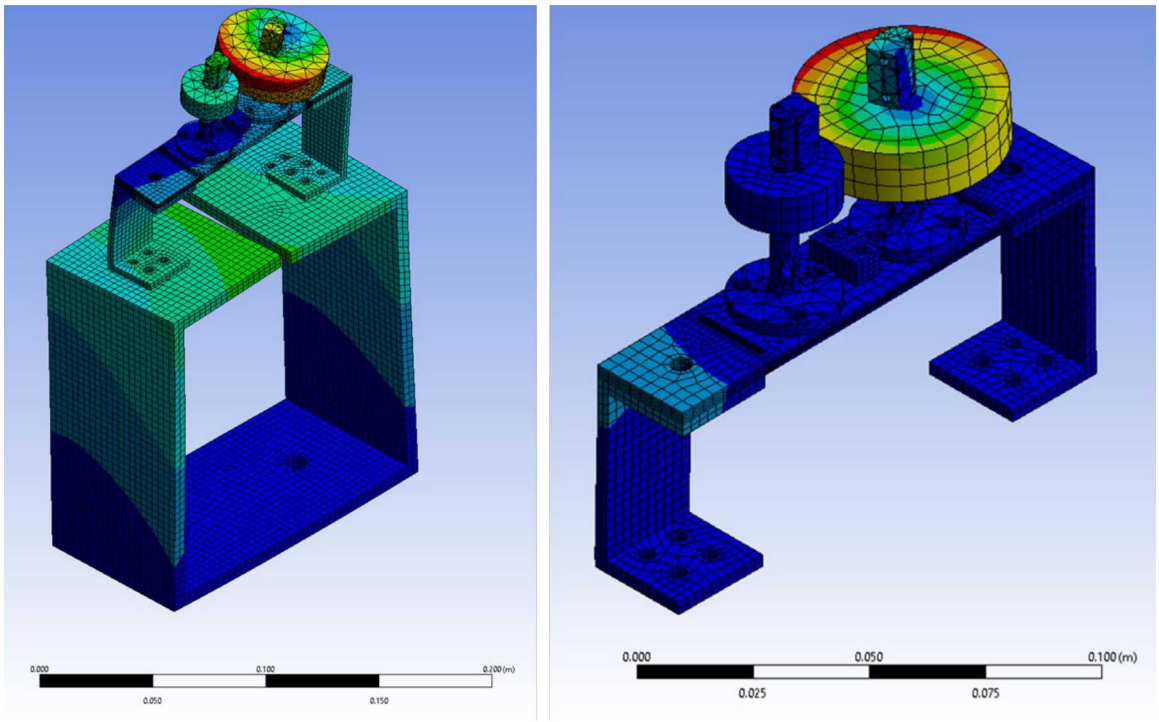

Figure 8: BOB Mode 5 [282 Hz] (left) and BRIDGE Mode 3 [326 Hz] (right)

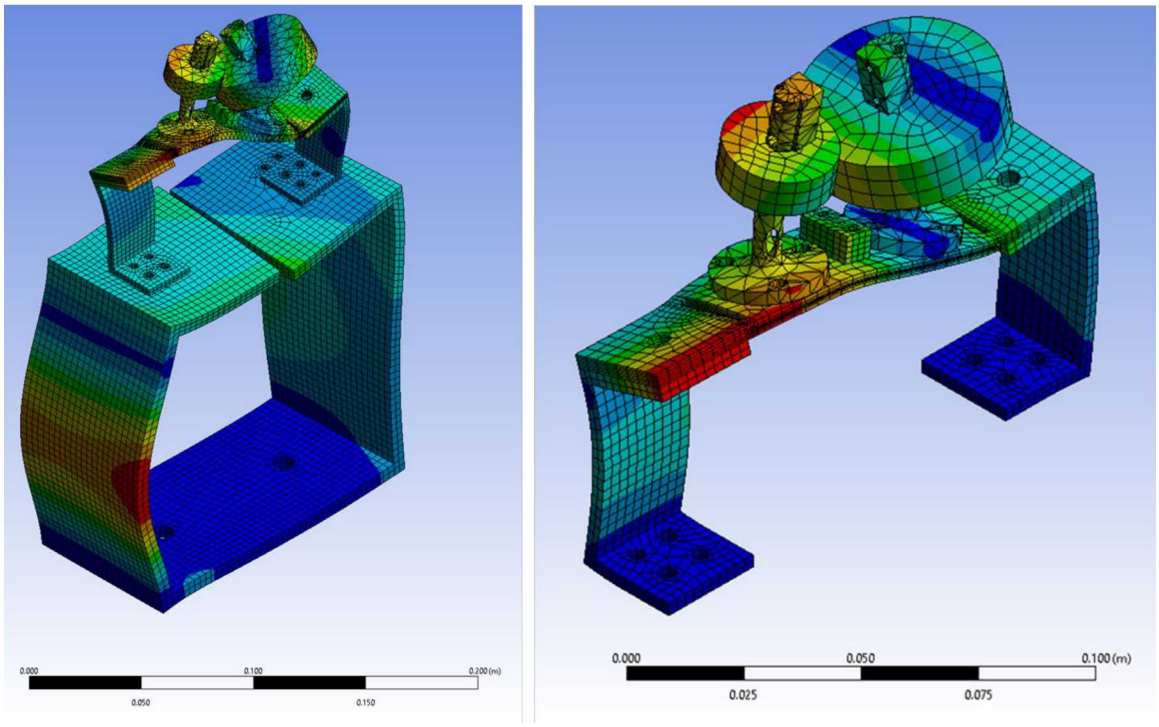

Figure 9: BOB Mode 20 [1480 Hz] (left) and BRIDGE Mode 11 [1561 Hz] (right)

III. DAMAGE RELATED QUANTITIES OF INTEREST

We want quantities of interest (QoIs) for which we can define threshold levels that give an indication of whether the shock environment is damaging. The quantities of interest in this study were:

A) peak acceleration measured at the towers;
B) peak relative displacement of the towers;
C) pseudo-velocity SRS using measured accelerations at the carriage and base of the bridge;

Physical damage, either fracture or plastic deformation, was qualitatively assessed through observation to define threshold levels of the QoIs. Figure 10 shows a typical damaged system. In this case, the tower with the large weight suffered permanent plastic deformation.

An important assumption that was made in this project is that the damaging effects of shocks are not cumulative when the response is in the elastic range. That means that shocks that do not cause plastic deformation or fracture are assumed to be non-damaging.

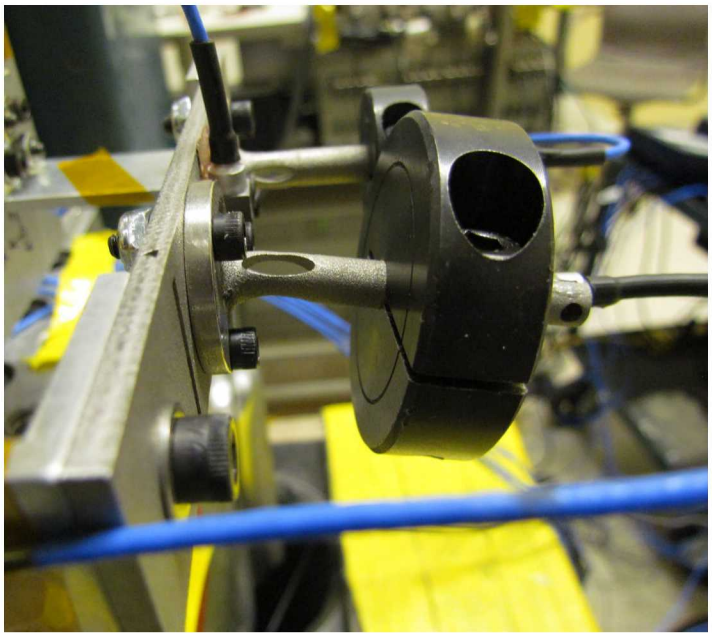

Figure 10 Example of Damage - Plastic Deformation of the Large Weight Tower

IV. TEST SETUP

The drop shock tests were conducted at Sandia National Laboratories Shock Laboratory with a MTS 12" Accelerated Drop Table. The bungee cords were removed so all tests were freefall tests. The first tests were characterization tests, such that the systems response to a small shock input could be observed below the yielding threshold. These characterization tests had less than a 100 G loading shock input into the assembly system. The duration was about 1 millisecond, and the drop height was about 2-inches. These tests were conducted for both test structures, with respect to all three primary axes: X, Y, and Z (Figure 11, Figure 12).

The other tests were failure tests. These tests were conducted with the intent of inducing large deformation or cracking within a component of interest. The G levels were above 400 G and lasted for 1 millisecond. The drop heights for these tests varied from 25 inches to 85 inches. The drop height for most tests was 40 inches or less. Only the Y-axis tests exceeded drop heights of 40 inches,

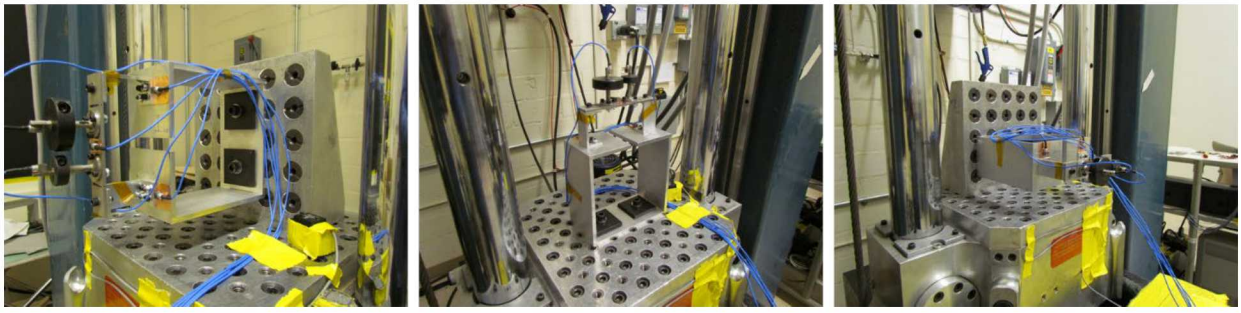

Figure 11: BOB Configuration, X-axis test (left), Y-axis test (middle), and Z-axis test (right)

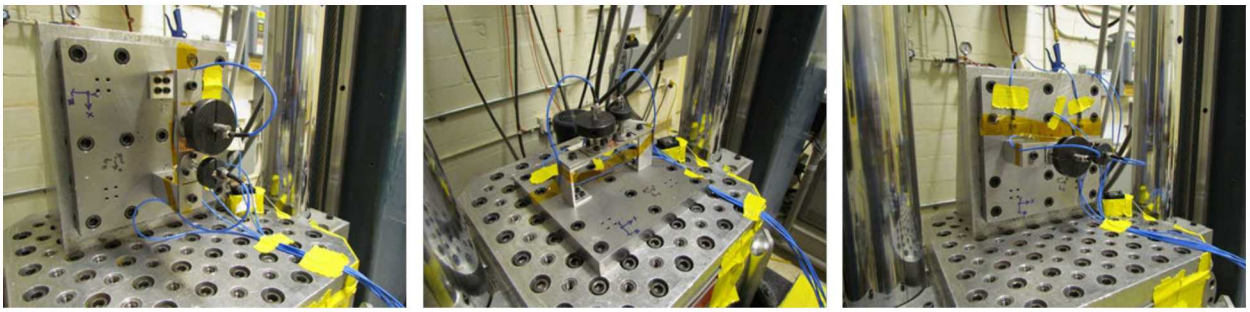

Figure 12: BRIDGE Configuration, X-axis test (left), Y-axis test (middle), and Z-axis test (right)

V. TEST RESULTS

Response at the Base of the Bridge

In Figure 13, four sets of data points are plotted against the carriage peak acceleration. There is also a line with a slope of one that starts at 400 G and ends at 600 G. Accelerations above this line represent an amplification of the shock at the base of the bridge relative to the shock measured on the carriage. Figure 13 shows that the BARC box in the BARBECUE test structure acts as a shock isolator, since all the points are below the green line. The points enclosed by ellipses indicate that failure occurred during the test. \

The Y-direction tests of the BRIDGE configuration showed no difference between the carriage's environment and the base of the Bridge's environment (Figure 14). The reason for this behavior is that the BRIDGE configuration was mounted to the fixture. The BARC box in the BOB configuration also acted as a shock isolator, just as in the X-direction.

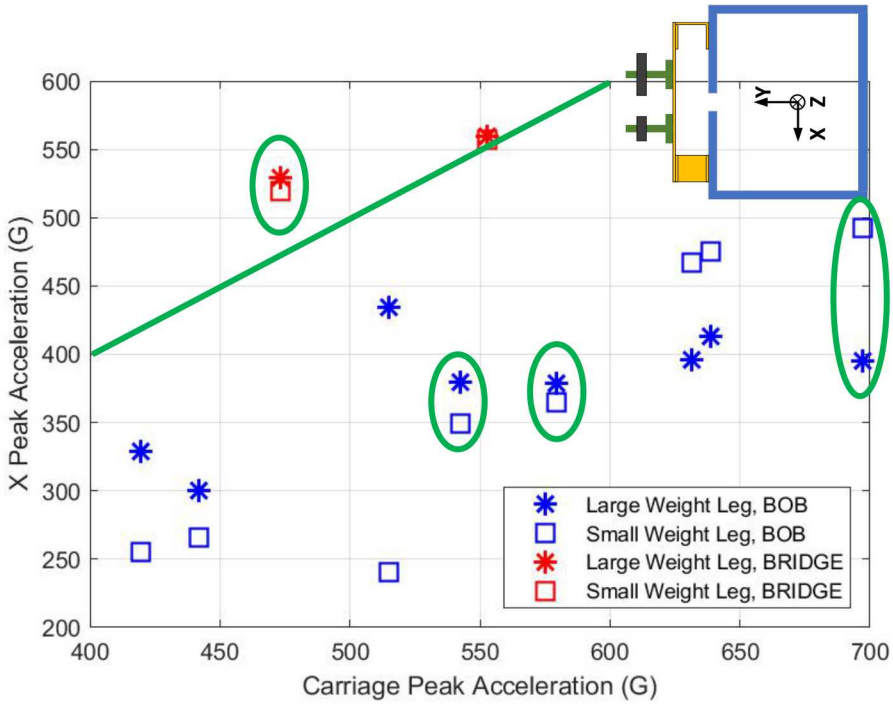

Figure 13: Base of Bridge Peak Accelerations v. Carriage Peak Acceleration [X-direction]

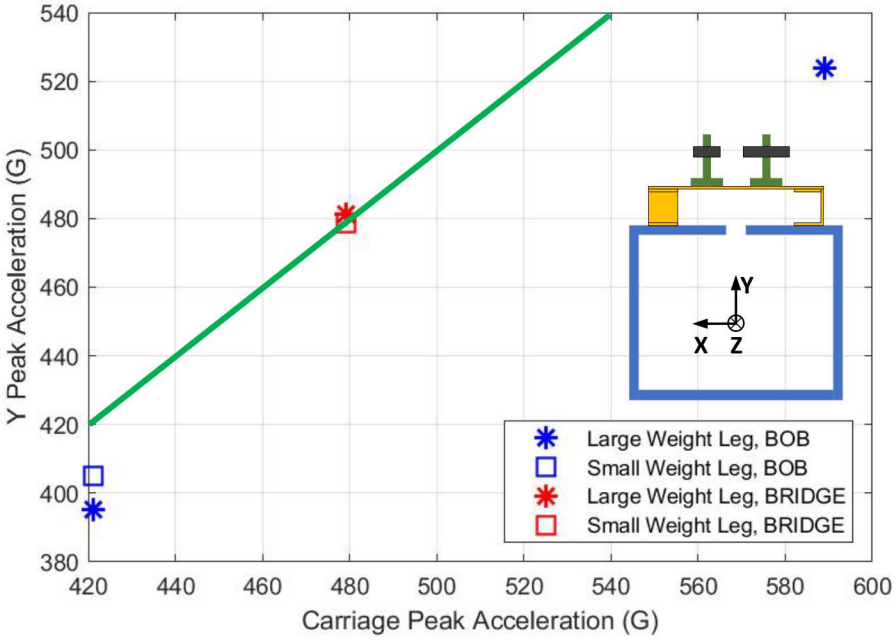

Figure 14: Base of Bridge Peak Accelerations v. Carriage Peak Acceleration [Y-direction]

Figure 15 shows that the accelerations measured at the base of the bridge on the small weight side are larger than those on the large weight side, and also higher than those on carriage in the BOB configuration. The accelerations on the large weight side are in family with, or lower than, the carriage peak acceleration. The reason for this difference was not determined. In the BRIDGE configuration the accelerations at the bridge base are higher than the accelerations measured on the carriage. This may be due to some compliance in the fixture (see Figure 12)

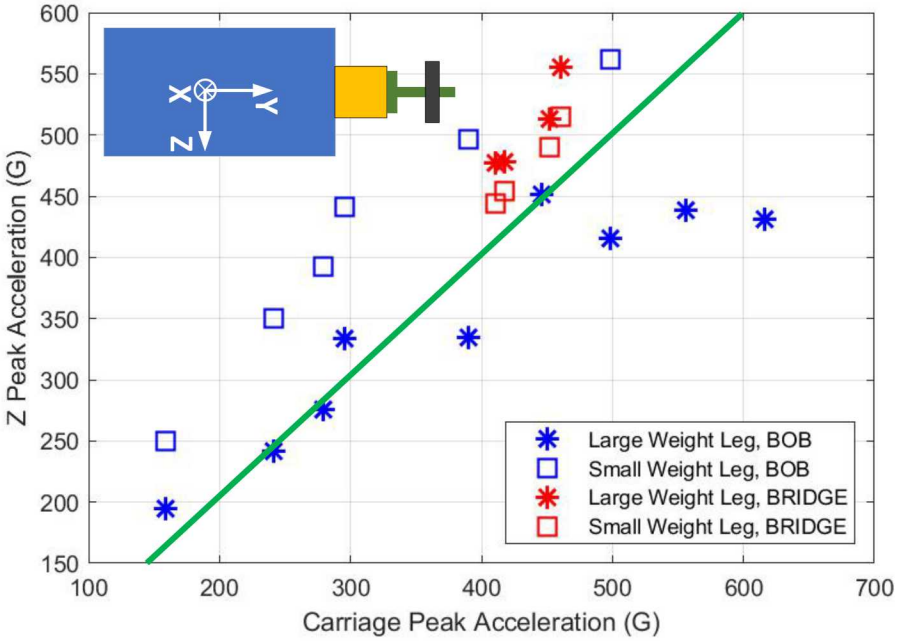

Figure 15: Base of Bridge Peak Accelerations v. Carriage Peak Acceleration [Z-direction]

Summary of Damage

Table 3 summarizes the damaging tests and the types of damage that the structure suffered. For Z-axis tests, the damaging shock levels are similar for both the BOB and BRIDGE configurations, and the type of damage is similar as well. The BRIDGE configuration was less robust than the BOB configuration in the X-axis and Y-axis tests. Generally, the BRIDGE configuration was damaged at lower shock levels than the BOB configuration. The BOB configuration was very robust in the Y-axis. There was no visible damage when it was dropped from 45" (707 G peak).

Table 3 Summary of Damaging Tests and the Damage Suffered

Configuration	Axis	Test	Drop Height	Carriage Peak G	Damage
BOB	Z	54	35"	445	Large Weight tower considerably bent Small Weight tower slightly bent
BRIDGE	Z	63	30"	451	Large Weight tower bent Small Weight tower slightly bent
BRIDGE	Z	66	30"	550	Large Weight tower bent Small Weight tower slightly bent
BOB	X	73	35"	542	Large Weight tower bent
BOB (same)	X	74	40"	639	Large Weight tower considerably bent Bridge crack on Small Weight side
BOB	X	77	35"	580	Large Weight tower bent Small Weight tower slightly bent
BRIDGE	X	68	25"	493	Large Weight tower considerably bent
BRIDGE	X	70	25"	472	Large Weight tower considerably bent
BOB	Y	82	45"	707	No damage
BRIDGE	Y	89	60"	719	Bridge bent on Small Weight side
BRIDGE (same)	Y	93	85"	1029	Bridge Small Weight side leg bent Large Weight tower buckled Bridge considerably bent on Small Weight side

Peak Accelerations at the Towers

The towers on the bridge were two components of interest so we wanted to understand the contribution of boundary conditions to their robustness to mechanical shocks. Figure 16 summarizes the peak accelerations measured at the tips of the two towers for the Z-axis shocks. In both configurations the accelerations were higher on the small weight tower – the red and blue squares are all higher than the red and blue stars in Figure 16. However, the large weight tower suffered more damage (Table 3). This is most likely because of the way the C-channels are oriented. The leg of the C-channel on the small weight side is parallel with the bridge (Figure 17), while the C-channel leg on the large weight side is perpendicular to the bridge span. The BARC box is stiffer in the Z-axis than the small weight side C-channel. This means that the C-channel on the small weight is the most compliant element in the load path for a Z-axis shock. Because the tower accelerometers are at the end of the towers the compliant leg will allow more motion and thus higher peak accelerations.

Since the large weight tower suffered more damage in the Z-axis tests, peak acceleration may not be a good predictor of damage potential when there is a compliant element in the load path. Another QoI, such as relative displacement across the component of interest may be a better predictive QoI when there is a flexible component in the load path. Indeed, in this test there was more displacement in the large weight tower (Figure 21).

The Y-axis results show a similar behavior. In this orientation, the weakest component was the inward facing C-channel leg. Figure 18 shows that the accelerations on the small weight tower are larger than those measured on the large weight tower in the BRIDGE configuration (i.e., the red squares are above the red stars). For the BOB configuration, the accelerations were higher on the large weight tower (i.e., the blue stars are above the blue boxes). In the BRIDGE configuration the small weight was on the side with the inward facing C-channel (Figure 19) and in the BOB configuration the large weight was on the side with the inward facing C-channel (Figure 20). The acceleration on the tower closest to the inward facing C-channel side was higher in both configurations.

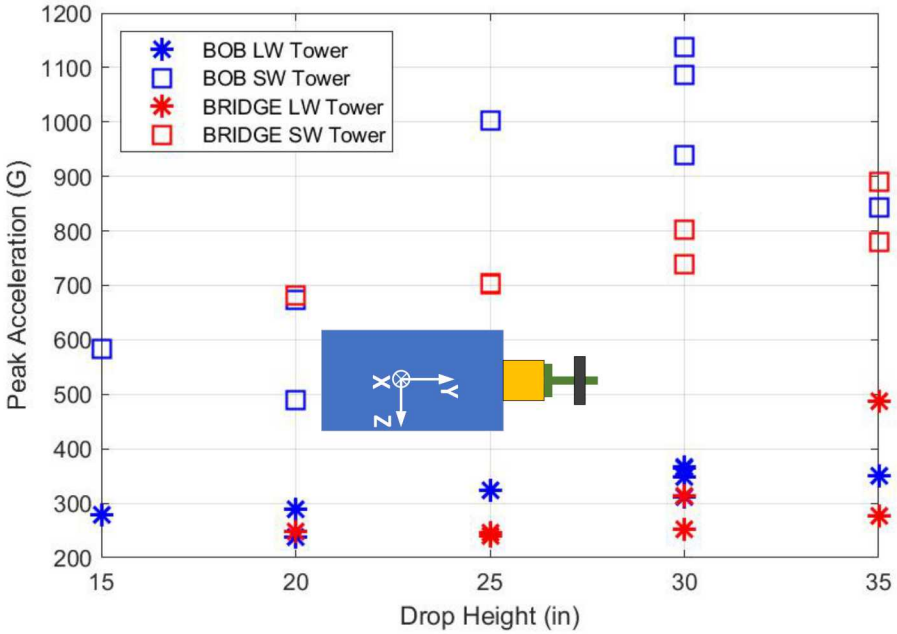

Figure 16 Peak Accelerations for Z-axis Shocks

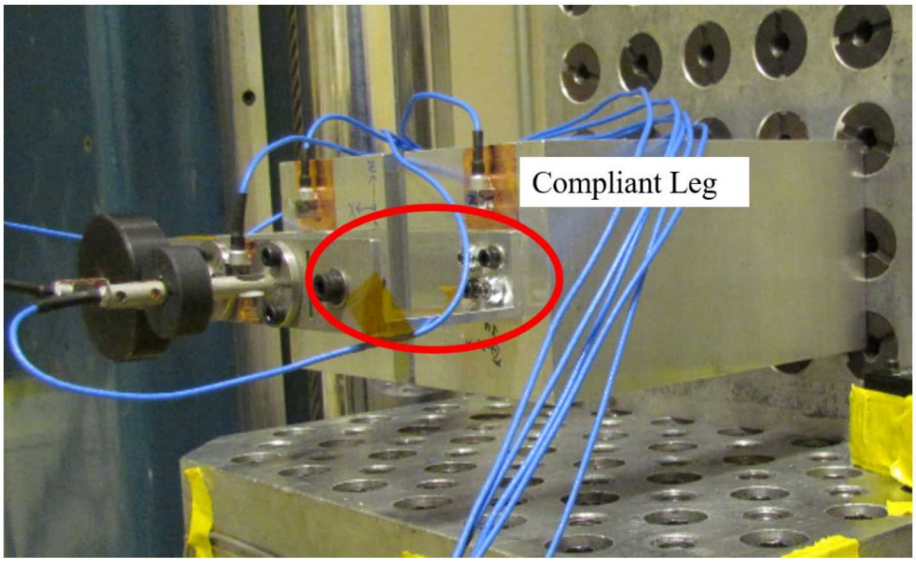

Figure 17 Compliant C-channel leg for Z-axis Shocks

In the BRIDGE configuration, the C-channel was damaged, and the measured accelerations were higher on that side. So, unlike the Z-axis shocks there is a correlation between high peak accelerations and damage. This is because the compliant component was also the least robust component. Had the large weight been on the tower on the inward facing C-channel side, the damage would likely have been worse.

The BOB configuration suffered no obvious damage from the Y-axis shocks. The peak accelerations were lower than those in the BRIDGE configuration for the same drop heights. This suggest that in the BARBEQUE configuration, the BARC box acted as a shock isolator for the Y-axis shocks.

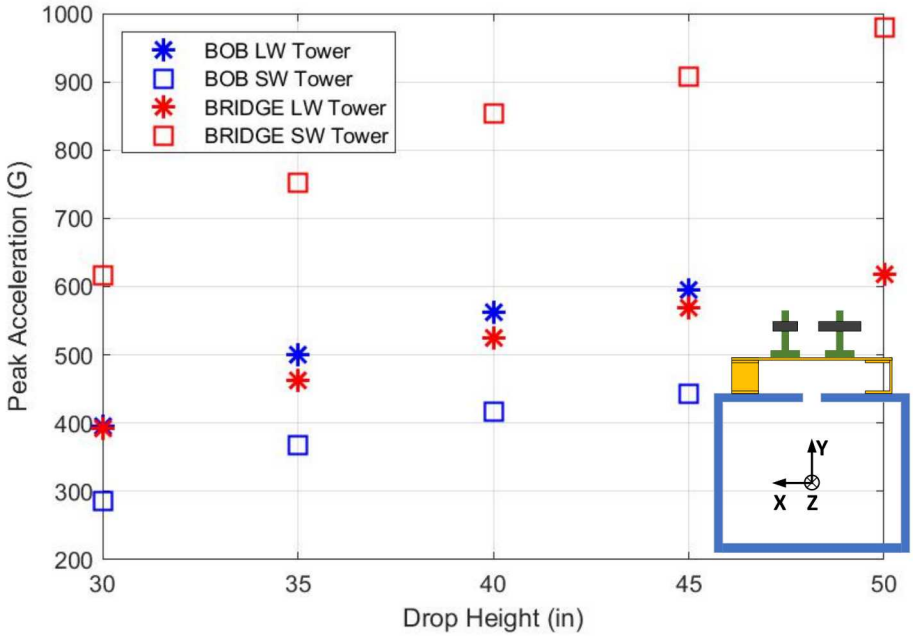

Figure 18 Peak Acceleration vs Drop Height for Y-axis Shocks

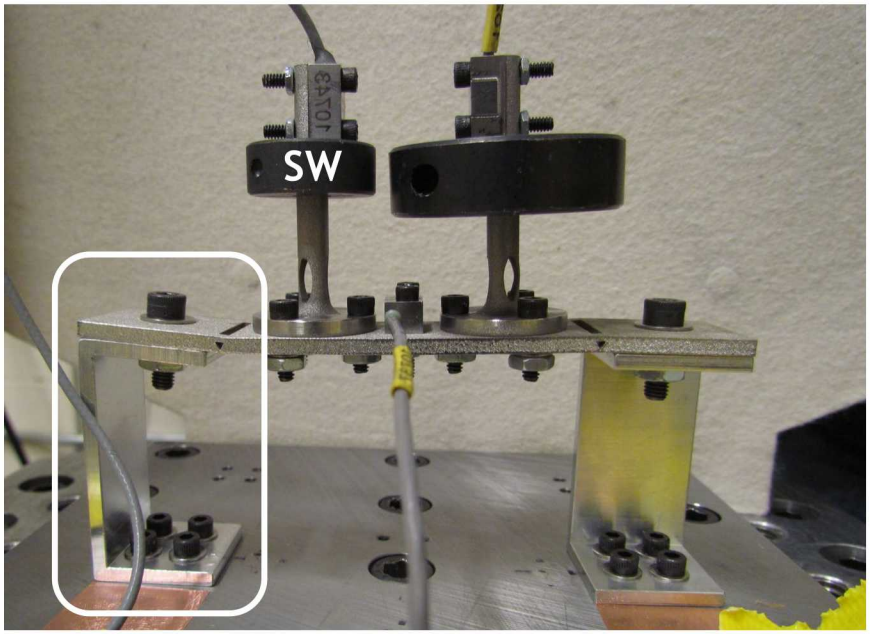

Figure 19 Y-axis BRIDGE Configuration - Damage to C-channel

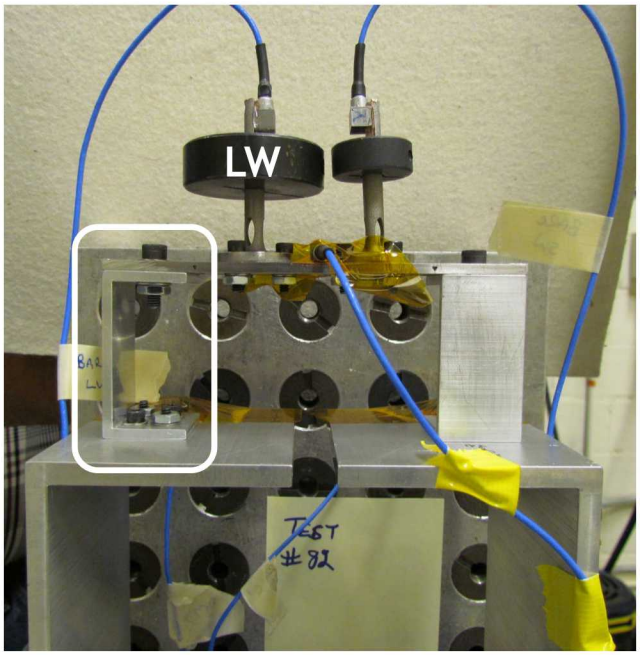

Figure 20 Y-axis BOB Configuration - No Damage

Relative Displacement

The relative displacement across a component is another QoI that can give insight into robustness to shock loading because it is related to stress. Strain-displacement relationships are well known [3]. One of the challenges with relative displacement is that it requires double integration of the measured accelerations. The integration operation is sensitive to measurement artifacts such as accelerometer drift and residual bias. Relative displacement was computed by first high-pass filtering the accelerations at 50 Hz. Then the filtered accelerations were integrated twice to obtain displacement. The displacements were subtracted to get the relative displacements, which were detrended to remove any residual drift.

The BOB configuration Z-axis tests were discussed in the section on peak acceleration. The relative displacements of each tower with respect to the bridge in Test 54 are shown in Figure 21. The relative displacement of the LW tower is larger than that of the SW tower. This is consistent with the observed damage shown in Figure 10.

The X-axis tests showed inconsistent relative displacements of the towers. The relative displacements of the two towers in X-axis Test 70 are shown in Figure 22. The displacement of the small weight tower is much larger than that of the tower with the large weight, but it was the large weight tower that suffered damage. Figure 23 shows the damaged state from Test 69 which was similar to the damaged state after Test 70.

Figure 24 shows the displacement of the bridge with respect to the average displacement at the base of the C-channel legs from two Y-axis tests in which the peak accelerations were comparable. The peak acceleration in the BOB configuration test was 665 G with a pulse duration of 0.96 msec. The drop height was 40". In the BRIDGE configuration test, the peak acceleration was 661 G with a pulse duration of 1.14 msec, and the drop height was 55". The peak magnitudes of the bridge relative displacements are comparable, and neither test caused any damage. None of the Y-axis tests of the BOB configuration caused any damage.

The relative displacements of the bridge for two BRIDGE configuration tests are shown in Figure 25. The peak relative displacement from Test 91 is about 38% higher than the peak relative displacement in Test 88. The C-channel bent in Test 91. This suggests that the minimum damaging drop height for the BRIDGE configuration is between 55" and 70" and less than 880 G. We did not perform any tests at the 880 G level with the BOB configuration.

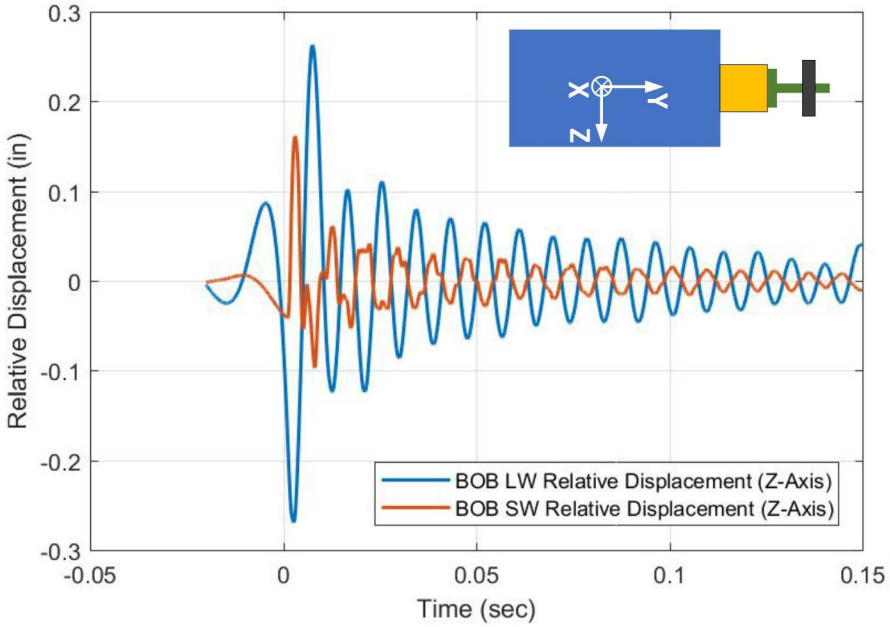

Figure 21 Relative Displacement of the Towers
(BOB Test 54 [35"/445 G/1.35 msec])

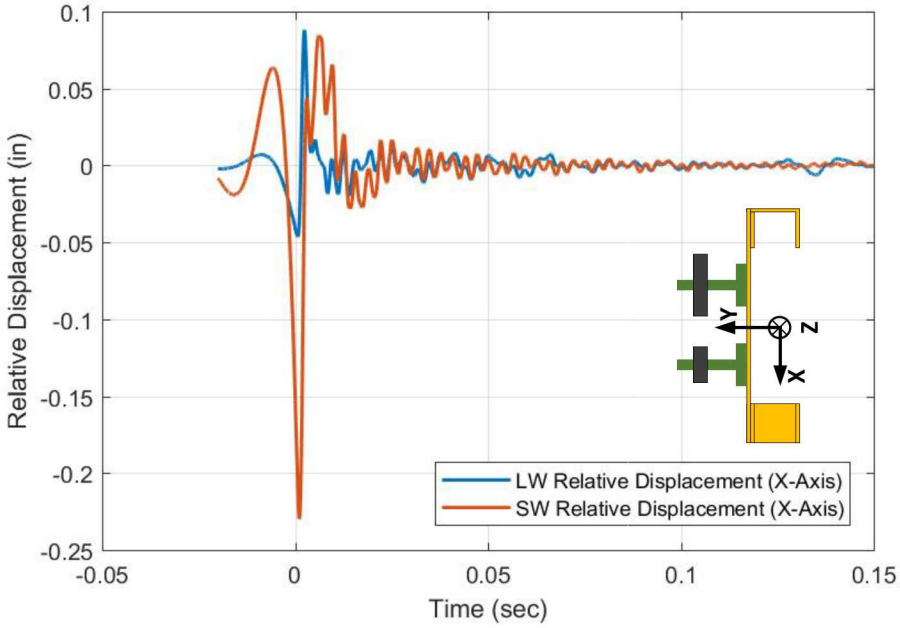

Figure 22 Relative Displacement of the Towers
(BRIDGE Test 70 [25"/472 G/0.91 msec])

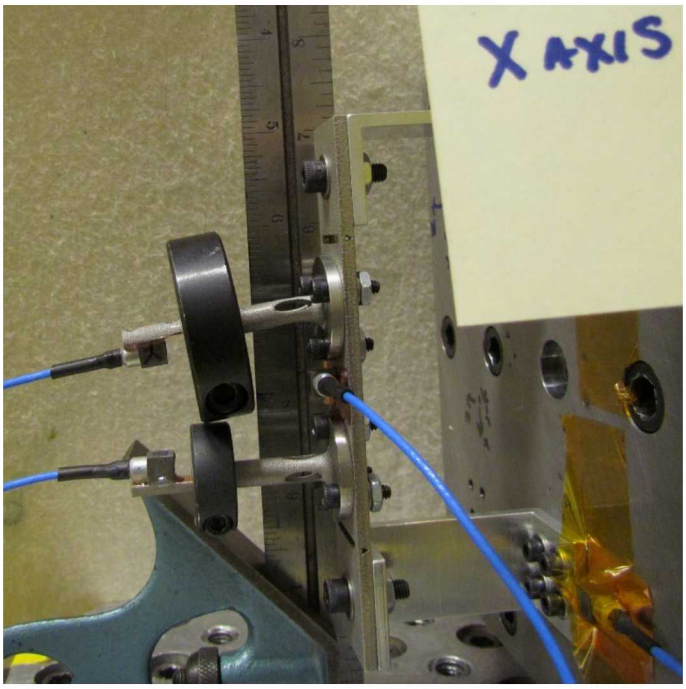

Figure 23 Deformed State of the BRIDGE Configuration after Test 69

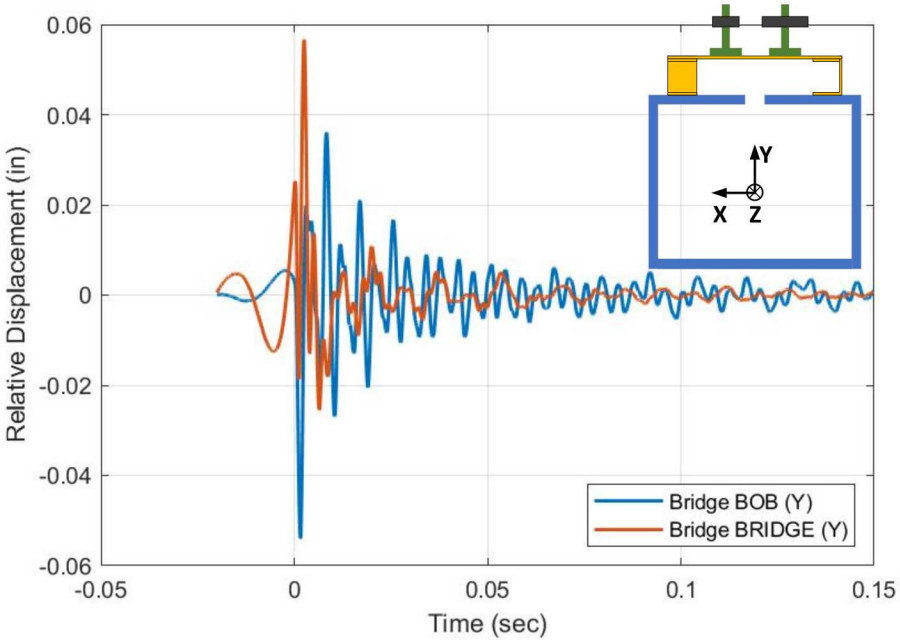

Figure 24 Relative Displacement at the Bridge
(BOB Test 81 [40”/665 G/0.96 msec]; BRIDGE Test 88 [55”/661 G/1.14 msec])

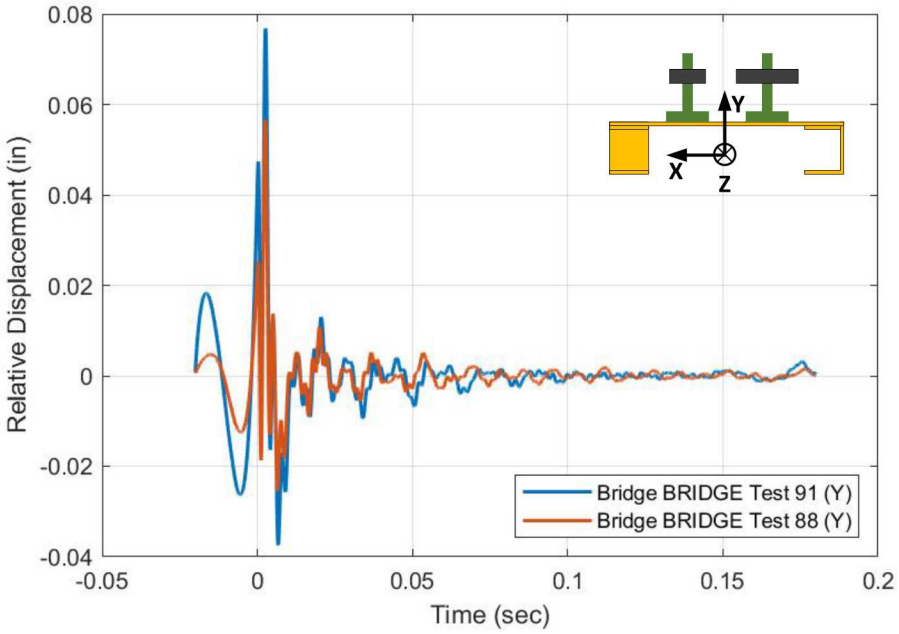

Figure 25 Relative Displacement at the Bridge
(BRIDGE Test 91 [70"/880 G/1.11 msec]; BRIDGE Test 88 [55"/661 G/1.14 msec])

Pseudo-Velocity Shock Response Spectra

Pseudo-velocity is related to strain and stress in linear systems [1]. We computed the pseudo-velocity SRS (PVSRS) using the accelerations measured at the base of the bridge. Accelerations from tests that caused damage in both configurations were used. Figure 26–Figure 28 show the PVSRS for shocks in each axis.

Figure 26 was created with accelerations from Test 54 (BOB configuration in which the Large Weight tower showed large plastic deformation) and Test 63 (BRIDGE configuration in which both towers were bent). The Y-axis PVSRS plots in Figure 27 were created from Test 79 (BOB configuration) and Test 83 (BRIDGE configuration). Neither test caused any damage to the structure and its components. In the X-axis shocks shown in Figure 28 (Test 73, BOB configuration; Test 69 BRIDGE configuration) the large weight tower bent in both tests. The figures show that the BOB environment at the base of the bridge is dynamically richer; however, the dynamics may not be the critical factor because damage in both configurations was consistent. This suggests that ΔV from the impact maybe more important than the vibratory response.

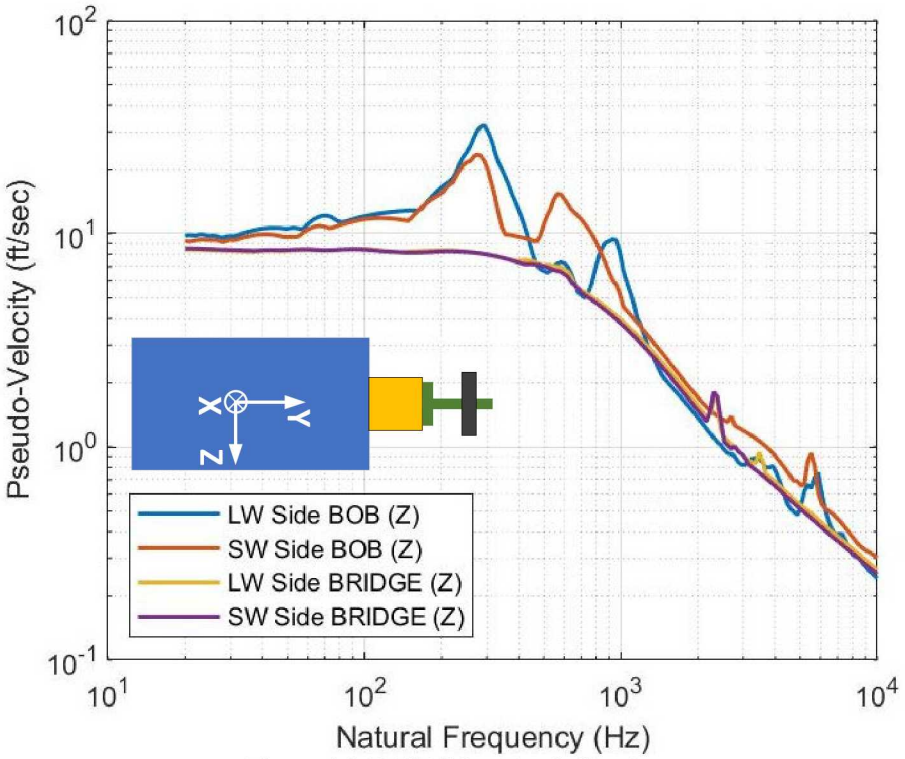

Figure 26 PVSRS for Z-axis Shocks
(BOB Test 54 [35”/445 G/1.35 msec]) BRIDGE Test 63 [30”/451 G/1.01 msec])

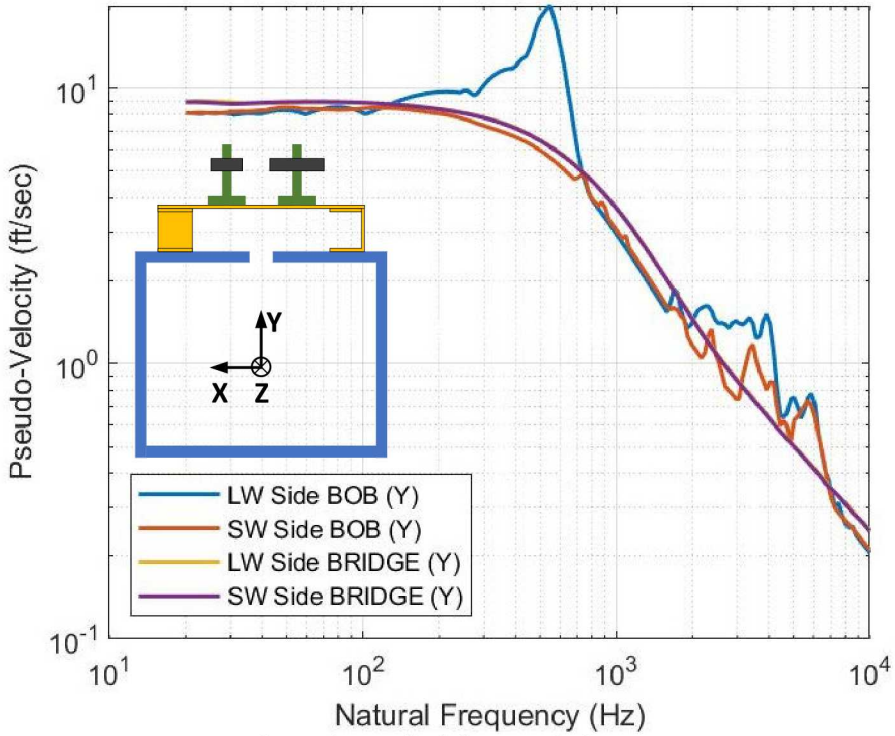

Figure 27 PVSRS for Y-axis Shocks
(BOB Test 79 [30”/420 G/1.07 msec]) BRIDGE Test 83 [30”/447 G/1.02 msec])

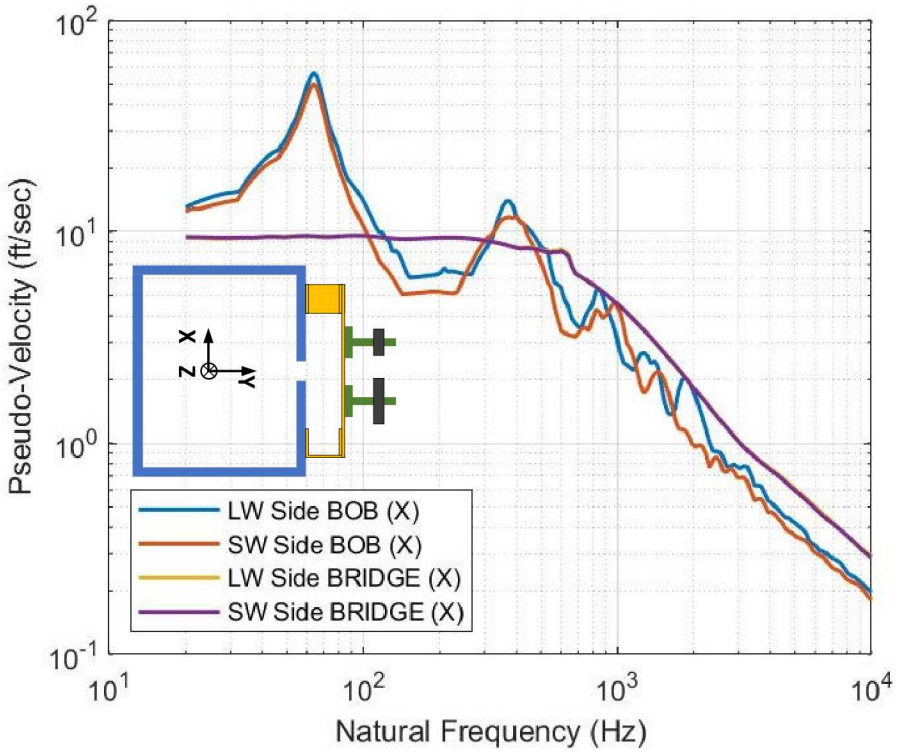

Figure 28 PVSRS for X-axis Shocks
(BOB Test 73 [35"/541 G/1.02 msec]) BRIDGE Test 69 [30"/550 G/0.92 msec])

VI. SUMMARY AND CONCLUSIONS

The objective of the work described in this paper was to investigate how boundary conditions may affect damage potential or component robustness to drop shock loads. We did this through experiments on two configurations of the BARBECUE testbed. The BARBECUE testbed is a variation on BARC testbed in that it has damage sensitive components. The damage sensitive components of interest were the two towers on the bridge. Differences in the boundary conditions at the base of the bridge resulted from the presence or absence of the BARC box.

Drop shock tests were carried out on both BARBECUE configurations in three axes individually. We found that damage sensitivity depends on geometry and the flexibility of components in the load path as much as on the boundary conditions. All three elements must be considered when evaluating damage to shock loading and quantities to represent the shock environments. In the Z-axis shocks, the BARC box was stiffer than the bridge so its presence was not critical to component robustness to drop shock events. The compliance of the C-channel bridge legs was more important. Similar, but less pronounced results were found for X-axis shocks. The boundary conditions were important in the Y-axis shocks. In this direction, the BARC box introduced flexibility into the load path so it acted as a shock isolator. This orientation gave the clearest manifestation of the importance of boundary conditions.

Peak acceleration is a popular quantity of interest to describe the severity of a shock environment. We found that peak acceleration at a component of interest may be misleading based on the geometry and flexibility of load path components. If there is flexible component in the load path, the accelerations may be high on the shock sensitive component but that may be due to non-damaging rigid body motion. This suggests that geometry and load paths should be considered when defining environments, instrumentation and quantities of interest. Relative deformational quantities of interest are likely to be more predictive, but their utility depends on good measurements since accelerations must be integrated.

REFERENCES

[1] Schoenherr, T., "Boundary Conditions in Environmental Testing Challenge Problem", Sandia National Laboratories, https://connect.sandia.gov/sites/TestBoundaryConditions.

[2] Soine, D.E., et al., "Designing Hardware for the Boundary Condition Round Robin Challenge," Paper 89, Proceedings of the 36th IMAC, Orlando, FL, Feb. 2018.

[3] Craig, R.R., *Mechanics of Materials*, John Wiley & Sons, New York, NY, ISBN 978-0470481813.

[4] Sisemore, C.L., and V. Babuska, *The Science and Engineering of Mechanical Shock*, Springer, 2020, ISBN 978-3-030-12102-2.